PHILOSOPHICAL TRANSACTIONS OF THE ROYAL SOCIETY A MATHEMATICAL, PHYSICAL & ENGINEERING SCIENCES

High–resolution maser studies of galactic nuclei

James M. Moran

Phil. Trans. R. Soc. Lond. A 2000 **358**, 797-810
doi: 10.1098/rsta.2000.0559

THE ROYAL SOCIETY

High-resolution maser studies of galactic nuclei

By James M. Moran

Harvard–Smithsonian Center for Astrophysics, 60 Garden Street, MS 42, Cambridge, MA 02138, USA

Water vapour masers are proving to be remarkably useful probes of the neutral accretion discs surrounding black holes at radii of a few tenths of a parsec. This paper describes the observational results on NGC 4258, including measurements of the magnetic field (less than 300 mG), the accelerations of the high-velocity features (-0.8 to $0.4\ \mathrm{km\,s^{-1}\,yr^{-1}}$), and the distance ($7.2 \pm 0.5$ Mpc). The status of measurements of other masers with resolved structure is also described.

Keywords: masers; black holes; magnetic fields

1. Preamble

Soon after the publication of our paper in *Nature* describing the distribution of the masers in the nucleus of NGC 4258 (also known as M 106), which suggested that they orbit a black hole of 40 million solar masses, I received a letter from Donald Lynden-Bell. It was dated 25 January 1995. In it he said, 'Your very remarkable discoveries concerning M 106 contained in the paper in *Nature* have given, at last, a convincing case of a dead quasar in a galactic nucleus.' He included a copy of John Michell's paper to The Royal Society in 1784, in which Michell speculated on the behaviour of light emanating from massive bodies. He concluded by saying, 'Your new method of distance determination is especially interesting and one wonders whether it will become the basis of good extragalactic distances once there are more objects in the years to come.' I am pleased to be at this meeting of The Royal Society, 215 years after the publication of Michell's paper, to describe the recent progress in the use of masers to study the environments of black holes and to determine their distances.

2. Introduction

The beautifully simple structure of the water vapour masers orbiting the nucleus of the nearby galaxy NGC 4258 was first described by Miyoshi *et al.* (1995). These observations were among the earliest ones performed with the Very Long Baseline Array (VLBA), which was dedicated in 1993. The success of these measurements relied on the versatility of that instrument, its angular resolution of 200 μas, and its excellent spectral resolution of less than 1 km s^{-1}. Since then, a series of 12 Very Long Baseline Interferometry (VLBI) experiments have been conducted by the group with members at the Harvard–Smithsonian Center for Astrophysics, the National Astronomical Observatory of Japan, the US National Radio Astronomy Observatory and the Max Planck Institute (MPI) for Radio Astronomy in Germany. This measurement program has been conducted with the VLBA, occasionally augmented by the

Table 1. *Parameters of molecular disc traced by water vapour masers in NGC 4258 and its associated black hole*[a]

inner radius, R_{i}	0.14 pc (3.9 mas)
outer radius, R_{o}	0.28 pc (8.0 mas)
inner rotation velocity, v_ϕ (R_{i})	$1100\ \mathrm{km\,s^{-1}}$
outer rotation velocity, v_ϕ (R_{o})	$770\ \mathrm{km\,s^{-1}}$
inner rotation period	800 yr
outer rotation period	2200 yr
position angle of disc (at 3.9 mas radius)	$80°$
inclination angle	$98°$
maser beam angle, β	$8°$
disc–galaxy angle[d]	$119°$
position-velocity slope	$282\ \mathrm{km\,s^{-1}\ mas^{-1}}$
central mass, M	$3.9\times10^{7}\ M_\odot$
Schwarzschild radius, R_{S}	1.2×10^{13} cm
Eddington luminosity	$5\times10^{45}\ \mathrm{erg\ s^{-1}}$
X-ray luminosity, L_{X}	$4\times10^{40}\ \mathrm{erg\ s^{-1}}$
apparent maser luminosity	$150\ L_\odot$
model luminosity[e]	$11\ L_\odot$
disc mass	$< 10^{6}\ M_\odot$
central mass density, uniform distribution	$> 4\times10^{9}\ M_\odot\ \mathrm{pc^{-3}}$
central mass, Plummer distribution	$> 10^{12}\ M_\odot\ \mathrm{pc^{-3}}$
centripetal acceleration, systemic features	$9.3\ \mathrm{km\ s^{-1}\ yr^{-1}}$
centripetal acceleration, high-velocity features	-0.8 to $0.4\ \mathrm{km\ s^{-1}\ yr^{-1}}$
disc systemic velocity[b], v_{o}	$476\ \mathrm{km\,s^{-1}}$
galactic systemic velocity (optical)[b,c]	$472\ \mathrm{km\,s^{-1}}$
radial drift velocity, v_{R}	$< 10\ \mathrm{km\,s^{-1}}$
thickness of disc, H	< 0.0003 pc
isothermal sound speed, T	< 1000 K
toroidal magnetic field, B	< 300 mG
distance, D	7.2 ± 0.5 Mpc

[a] Based on the distance estimate of 7.2 Mpc.
[b] Radio definition, with respect to the local standard of rest. To convert to heliocentric velocity (radio), subtract $8.2\ \mathrm{km\,s^{-1}}$; to convert to heliocentric (optical), subtract $7.5\ \mathrm{km\,s^{-1}}$.
[c] From Cecil *et al.* (1992).
[d] Angle between the spin axis of the molecular disc and the spin axis of the galaxy.
[e] Radiation into a zone within $\pm4°$ of the plane of the disc.

Very Large Array (VLA) and the MPI 100 m telescope to improve sensitivity. The observational results on NGC 4258 obtained over the past few years were reviewed in some detail by Moran *et al.* (2000). The interpretation of the data can be summarized briefly as follows (see table 1 for a list of parameters).

(1) The masers appear to trace a highly elongated, although slightly curved, structure (figure 1). The high-velocity redshifted and blue-shifted features are symmetrically offset in position on either side of the systemic features. The line-of-sight velocities, v, of the high-velocity features as a function of impact parameter b (position along the major axis of the distribution) follow the prediction of Kepler's third law of orbital motion, $v=\sqrt{GM/b}$, where G is the gravitational constant and M is

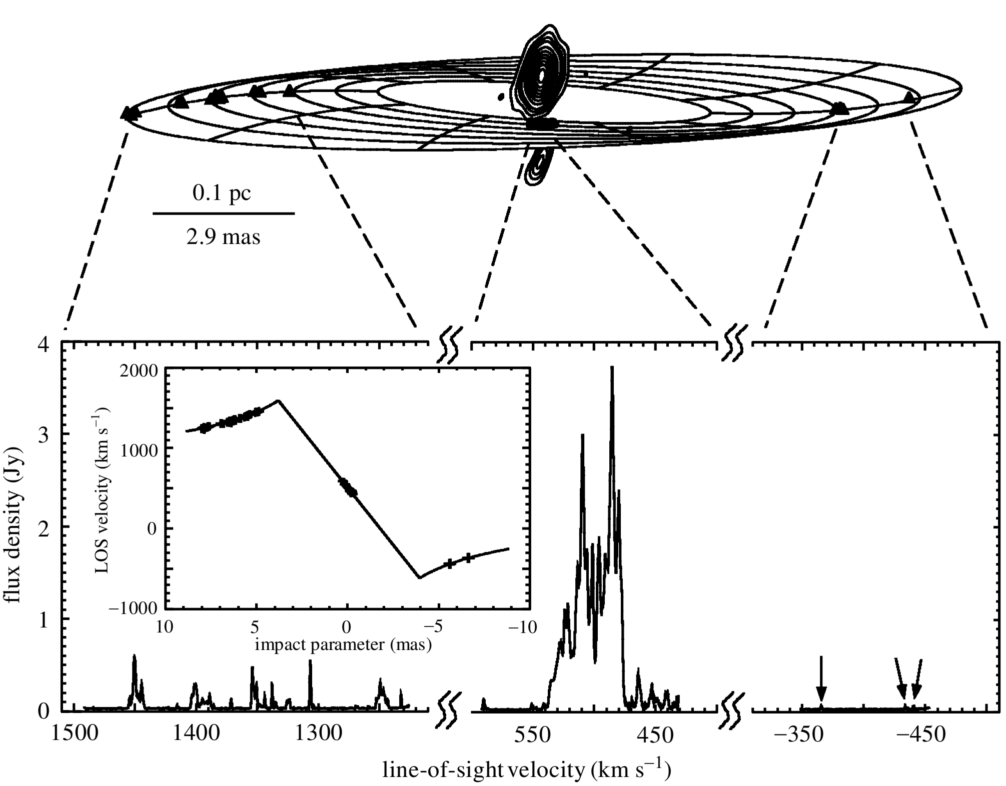

Figure 1. The top panel shows the positions of the water vapour masers, measured with VLBI. The linear scale is based on a distance of 7.2 Mpc. A warped disc that fits all the measurements is superimposed (wire grid). The dynamical centre of the system is marked with a filled square. The contours near the centre of the disc show the intensity of the continuum emission at 1.3 cm wavelength. The lower panel shows the spectrum of the maser. The velocity axis is based on the radio definition for Doppler shift and is referred to as the local standard of rest. There is no detectable emission in the omitted portions of the spectrum. The inset to the lower panel shows the line-of-sight velocity of the masers as a function of offset from the dynamical centre. From Herrnstein *et al.* (1999).

the central mass. The systemic features show a linear dependence with the impact parameter, suggesting that they are in circular orbital motion and are confined to a small annular region of radius R, where $R = (GM/v^2)^{1/3}b$. Detailed analysis of the system shows that the disc has an inclination angle of 98° (close to edge-on) and the high-velocity features lie on the midline (the diameter in the disc perpendicular to the line of sight), as described under item (4) below. With these parameters and with a distance of 7.2 Mpc, the required central mass is $3.9 \times 10^7\ M_{\odot}$. This mass is presumed to be a black hole. The Schwarzschild radius, R_S, is 1.2×10^{13} cm, and the Eddington luminosity is 5×10^{45} erg s^{-1}. The X-ray luminosity is only 4×10^{40} erg s^{-1} (Makishima *et al.* 1994) and the total luminosity is probably *ca.* 10^{42} erg s^{-1}. The mass density enclosed within a spherical volume inside the inner cut-off of the maser disc is $4 \times 10^9\ M_{\odot}$ pc^{-3} (Miyoshi *et al.* 1995).

(2) The distribution of maser features in the direction normal to the major axis is too small to be measured at present (see figure 2). The upper limit on the ratio

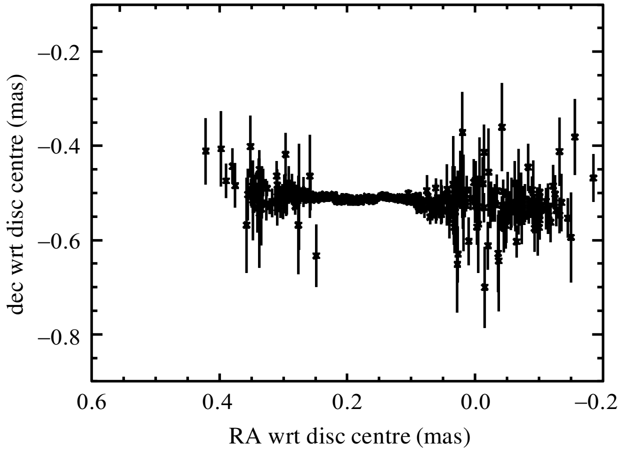

Figure 2. The positions of the systemic masers as a function of distance from the axis of the disc.

of thickness to radius of the disc is 0.0025 (Moran *et al*. 1995). If the masers trace the full vertical extent of the disc and the disc is in hydrostatic equilibrium, then either the sound speed or the Alfvén speed must be less than 2.5 $\mathrm{km\,s^{-1}}$ in the cases of thermal and magnetic support, respectively. This corresponds to a temperature of less than 1000 K, or a magnetic field strength of less than 100 mG.

(3) The upper limit of any toroidal component of the magnetic field in the maser medium, derived from a search for the Zeeman splitting of the maser feature at 1306 $\mathrm{km\,s^{-1}}$, is less than 300 mG (figure 3) (Herrnstein *et al*. 1998*a*). For pressure equilibrium between magnetic and thermal forces, the hydrogen number density in the disc would be less than $2 \times 10^{10}\ \mathrm{cm^{-3}}$. This is close to the density at which collisions are expected to thermalize the maser levels and quench the emission.

(4) The accelerations (i.e. the linear drift in the line-of-sight velocity with time) of the systemic features are *ca.* 9 $\mathrm{km\,s^{-1}\,yr^{-1}}$ (Haschick *et al*. 1994; Greenhill *et al*. 1995; Nakai *et al*. 1995). These accelerations support the Keplerian model and constrain the distance to the source. The high-velocity features that have been tracked have accelerations in the range of −0.8 to 0.4 $\mathrm{km\,s^{-1}\,yr^{-1}}$ (Bragg *et al*. 2000). These measurements constrain these masers to lie within 10° of the midline. The precise values of these accelerations can be used to determine the exact azimuthal positions of the masers in the disc.

(5) There is an elongated continuum radio source, which appears to be a bipolar jet emanating from the black-hole position, parallel to the axis of rotation of the disc (see figure 1) (Herrnstein *et al*. 1997). Careful removal of the jet emission from the continuum images shows that there is no 1.35 cm wavelength emission from the position of the black hole at the level of *ca.* 200 μJy (Herrnstein *et al*. 1998*b*). Any emission from an electron plasma of 10^9 K associated with an advection flow or corona must come from a region smaller than $100R_\mathrm{S}$. The continuum image was made from interferometry data that were phase-referenced to the maser data. Thus, the continuum image is correctly registered on the image of the maser emission to within 100 μas. Furthermore, the origin of the continuum emission is aligned with the dynamical centre of the disc. Hence any orbital ellipticity is small, except for a small parameter space where the major axis is nearly aligned with the line of sight.

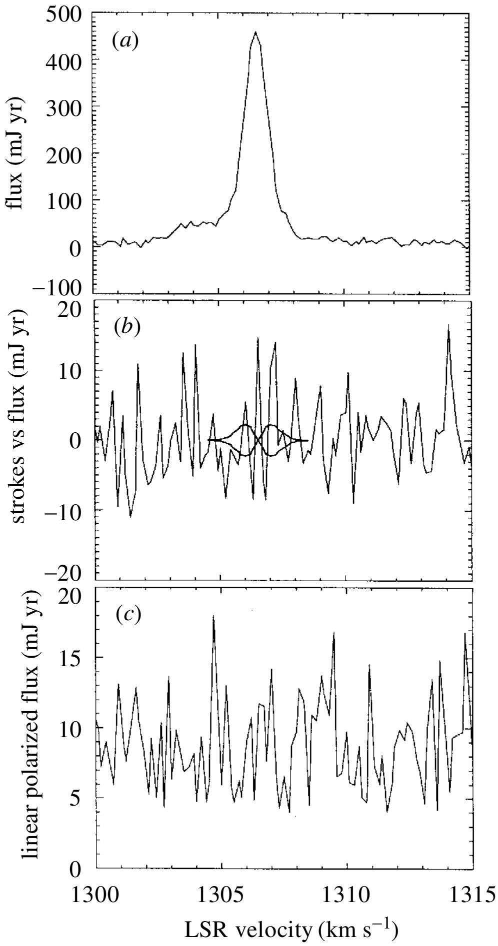

Figure 3. The search for the Zeeman splitting of the maser feature at 1306 km s^{-1} in NGC 4258 with the VLA. (*a*) The total intensity spectrum (Stokes parameter I). (*b*) The difference of spectra measured in circular polarization (Stokes parameter V). The Zeeman profiles corresponding to the $1-\sigma$ limit on the magnetic field are superimposed. (*c*) The linear polarization (Stokes Q^2+U^2). Note that the noise bias has not been removed, but there is no detectable linear polarization.

(6) The high-velocity features show no detectable proper motions with respect to a fixed-velocity component in the systemic range (Herrnstein 1996), as expected from their positions in the disc. The systemic features show proper motions of *ca.* 32 μas yr^{-1} (Herrnstein *et al.* 1999). The proper motions and the acceleration of the systemic features both give a distance of 7.2 Mpc.

Even though the masers are distributed in a zone between 40 000 and 80 000 $R_{\rm S}$, it may be possible to detect relativistic effects. The gravitational red shift and transverse Doppler shift are *ca.* 4 km s^{-1} (detectable), the expected Lense–Thirring precession (see below) is less than *ca.* 3° over the maser annulus (possibly detectable) and the apparent shift of the maser positions due to gravitational bending is *ca.* 0.1 μas (undetectable).

3. Magnetic field

It may be possible to determine the magnetic field in the maser clumps through the Zeeman effect. Unfortunately, water is a non-paramagnetic molecule, and the splitting is only 1 Hz mG^{-1}. Since the line widths are *ca.* 1 km s^{-1}, a field strength of *ca.* 75 G is required to produce a splitting equal to the line width. For small magnetic fields (less than 1 G), the Zeeman effect manifests itself as a small displacement of the left- and right-circularly polarized components. The line shape for the difference in circularly polarized spectra, Stokes parameter V, is proportional to the derivative of the line profile, which has a characteristic S-shaped signature. In other words,

$$V(v) = \frac{I_o \Delta v_z \cos\theta}{\sigma_d^2} v e^{-v^2/2\sigma_d^2}, \tag{3.1}$$

where I_o is the amplitude of the line, Δv_z is the Zeeman splitting in units of velocity, v is the offset in velocity from the line centre, σ_d is the line width and θ is the angle between the line of sight and the magnetic-field direction. Hence, the width of the profile is independent of the magnetic field, but the amplitude is proportional to the magnitude of the line-of-sight component (not the total magnitude) of the magnetic field. Measurement of the magnetic field requires very high sensitivity, and great care must be exercised to eliminate systematic effects that could produce false positive results. This technique has been used to convincingly detect magnetic fields in galactic water masers associated with star-forming regions (Fiebig & Güsten 1989). These fields are typically 100 mG for regions where the hydrogen number density is thought to be *ca.* 10^{10} cm^{-3}.

The 1306 km s^{-1} feature, which is the most isolated feature in the spectrum (see figure 1), was observed for 8 h with the VLA by Herrnstein *et al.* (1996). The spectra obtained are shown in figure 3. The limit on the fractional circular polarization was *ca.* 1%. Hence, the Zeeman effect was not detected, and the toroidal component ($\theta = 0$) of the magnetic field must be less than 300 mG. There are some caveats to this limit. There are three major hyperfine transitions in the maser transition; which one or ones are responsible for the maser emission is not known (see Moran *et al.* 1973; Walker 1984). The usual assumption is that the strongest line ($F = 7 \rightarrow 6$ hyperfine transition) is seen. There can be unusual radiative transfer effects in masers, but these usually lead to false positive Zeeman detections. No linear polarization was found, which for some specific maser theories (see, for example, Nedoluha & Watson 1992) leads to an upper limit of *ca.* 80 mG on the magnetic-field component perpendicular to the line of sight.

From the limit of 300 mG, and a temperature of 1000 K, we deduce a hydrogen number density, n, of 2×10^{10} cm^{-3} on the assumption of thermal and magnetic-field pressure balance, $nkT = B^2/8\pi$, where k is Boltzmann's constant, B is the magnetic field and T is the temperature of the maser gas. This is close to the maximum allowable hydrogen density in a water maser of *ca.* 10^{10} cm^{-3}, based on thermalization by water levels via collisions. From the standard Shakura–Sunyaev model (Shakura & Sunyaev 1973; Frank *et al.* 1992), the inward drift velocity in the accretion disc is $v_R = \alpha v_\phi (H/R)^2$, where α ($\leqslant 1$) is the viscosity parameter, v_ϕ is the Keplerian velocity and H is the thickness of the disc at radius R. We can estimate the mass accretion rate based on the assumption of equipartition of energy and the Shakura–Sunyaev estimate of $v_{\rm R}$ as

$$\dot{M} \cong \frac{c_{\rm s} B^2 R^3 \alpha}{GM}, \qquad (3.2)$$

where $c_{\rm s}$ is the sound speed and R is the radius of the maser for which B was measured. For $c_{\rm s} = 2.5\ {\rm km\,s^{-1}}$, $B = 300$ mG at $R = 0.2$ pc and $M = 3.9 \times 10^7\ M_{\odot}$, the limit is

$$\dot{M} < 0.015\alpha\ M_{\odot}\ {\rm yr^{-1}}. \qquad (3.3)$$

Detailed theoretical modelling can give estimates for the accretion rate. For example, a model in which the cause of the outer radial cut-off in maser emission is attributed to the transition from molecular to atomic gas leads to an estimate of $10^{-4}\alpha\ M_{\odot}\ {\rm yr^{-1}}$ (Neufeld & Maloney 1995). Gammie *et al.* (1999) favour an accretion rate of $10^{-1}\alpha\ M_{\odot}\ {\rm yr^{-1}}$, based on an analysis of the continuum radiation spectrum. If the accretion rate is this high, then the relative weakness of the continuum radiation may be due to the process of advection (Gammie *et al.* 1999). On the other hand, if the accretion rate is low, then the weak emission is due to the dearth of infalling material. In this case the gravitational power in the accretion flow may be insufficient to power the jets.

Much better Zeeman experiments can be expected in the future. The proposed VLA upgrade will include a spectral correlator of much greater capacity, which will enable many lines to be observed at once (e.g. 10, see figure 1), and the system temperatures will be improved by a factor of about four. Hence, the noise could be reduced by a factor of about 20 for a 24 h integration, compared with the 8 h measurement of Herrnstein *et al.* (1998*a*). A magnetic field could be detected down to a level of 15 mG. If no field were detected, the limit on the estimate of the accretion rate would be reduced by a factor of 400 from that given by equation (3.3). Radial magnetic fields could be detected by a Zeeman experiment on the systemic-velocity masers.

4. Accelerations

It has been known for some time that the accelerations of the high-velocity features are small with respect to those of the systemic features ($9\ {\rm km\ s^{-1}\ yr^{-1}}$). Greenhill *et al.* (1995) and Nakai *et al.* (1995) put limits on any accelerations of *ca.* $1\ {\rm km\ s^{-1}\ yr^{-1}}$. More recently, Bragg *et al.* (2000) were able to track the velocities of 19 high-velocity features over a period of three years and determined their accelerations. These range from -0.4 to $0.8\ {\rm km\ s^{-1}\ yr^{-1}}$. Examples of the velocity drifts of the 1303 and 1306 ${\rm km\,s^{-1}}$ features are shown in figure 4. The median of the distribution of accelerations is close to zero, suggesting that the masers are clustered around the midline. From the nearly edge-on disc model, the azimuth angles with respect to the midline of the features can be estimated (without direct knowledge of their radii) by the equation

$$\phi \approx \frac{GMa}{(v - v_{\rm o})^4}, \qquad (4.1)$$

where v and a are the line-of-sight components of the velocity and acceleration, respectively, and $v_{\rm o}$ is the systemic velocity.

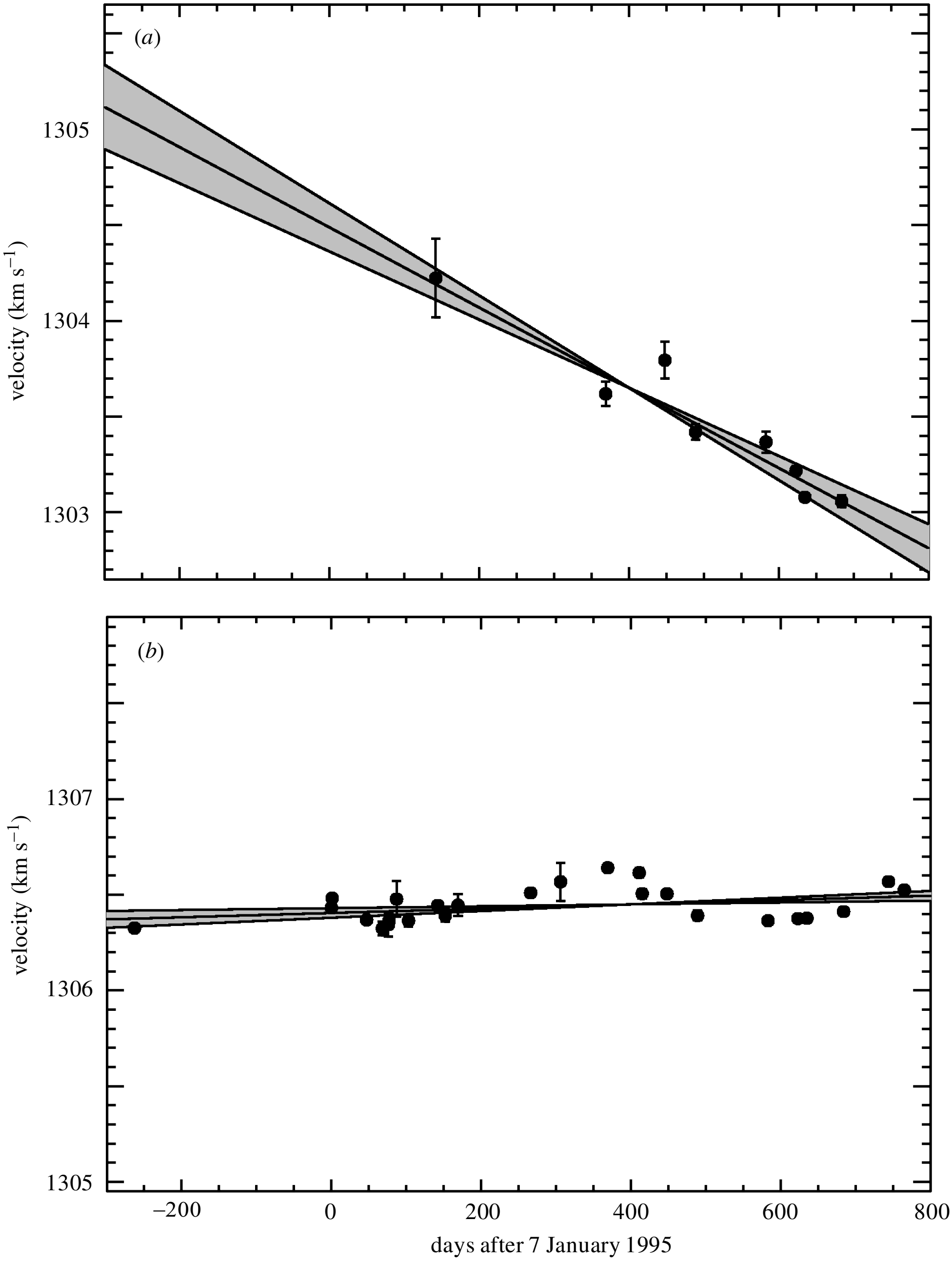

Figure 4. (a) The velocity centroid of the 1303 km s^{-1} feature as a function of time. The best-fitting straight line is shown with its errors. The acceleration of -0.765 ± 0.115 km s^{-1} yr^{-1} places this feature at a position 14° behind the midline in the context of the model of a nearly edge-on Keplerian disc. (b) The velocity centroid of the 1306 km s^{-1} feature. The acceleration of 0.041 ± 0.023 km s^{-1} yr^{-1} places this feature at a position 1° in front of the midline (Bragg *et al.* 2000).

Bragg *et al.* (2000) also found that, on average, the strongest high-velocity masers lie closest to the midline. This result is reasonable, since the line-of-sight velocity gradient is zero on the midline, so the potential amplification path length is greatest there. However, since the maser emission is dominated by discrete clumps of gas that give rise to identifiable velocity features, the importance of the velocity gradients is not obvious. Because the velocity gradient is smallest at the midline, the probability that two masers lined up along our line of sight will have nearly the same velocity is greatest there. Such aligned masers behave like long filamentary masers. Their emission is highly beamed and their observed strengths can be greatly enhanced compared with the individual strengths (Deguchi & Watson 1989).

5. Distance

The distance to the masers can be estimated from the disc model and measurements of either the accelerations or the proper motions of the systemic features. Fifteen features were tracked over a period of two years to an accuracy of 0.5–10 μas in relative position and 0.3 $\mathrm{km\,s^{-1}\,yr^{-1}}$ in acceleration (Herrnstein *et al.* 1999). The distance estimate derived from these numbers is based on simple geometric considerations. The Keplerian curve of the high-velocity masers gives the mass function $GM\sin^2 i/D$, where i is the inclination of the disc to the line of sight and D is the distance. The radius, R, of the systemic masers (in angular units) is determined from the slope of the velocity versus impact parameter curve shown in figure 1 (inset). This fixes the angular velocity, v_ϕ, of the systemic masers under the assumption that the orbits are circular. The expected accelerations and proper motions of the systemic features are v_ϕ^2/R and v_ϕ/D, respectively. The data for the features that could be reliably tracked are shown in figure 5. The distance to the maser determined from analysis of the proper motions and accelerations of the systemic features is 7.2 ± 0.5 Mpc (Herrnstein *et al.* 1999). The error includes an allowance for a possible eccentricity in the orbits of up to 0.1. The assumption that the orbits are circular or nearly circular is reasonable on theoretical grounds because of viscous relaxation, and on observational grounds because the continuum emission arises close to the centre of symmetry of the maser distribution.

Maoz *et al.* (1999) report a distance to a set of 15 Cepheid variables in NGC 4258 of 8.1 ± 0.8 Mpc. Their error is composed of a statistical error of 0.4 Mpc and the Hubble Key Project systematic error estimate of 0.7 Mpc. The largest component in this error term is the estimate by the Key Project team of the distance to the Large Magellanic Clouds (LMCs), 50 ± 4 kpc (Madore *et al.* 1999). Reducing the distance of the LMC estimate to 44.6 kpc would reconcile the maser and Cepheid scales and bring it close to the distance estimate obtained from the promising new red clump technique, 43.3 ± 1.2 kpc (see, for example, Stanek *et al.* 2000). Such a rescaling would raise the Hubble constant, as determined by the Hubble Key Project, by 12%.

6. The warp of the disc

Since the masers are distributed in the disc so selectively, it is difficult to determine the shape of the warp uniquely and precisely. It seems unlikely that features will be detected in other portions of the disc at present sensitivity levels. Better measurements of the positions and directions of motion of the high-velocity features are key to defining the warp more accurately.

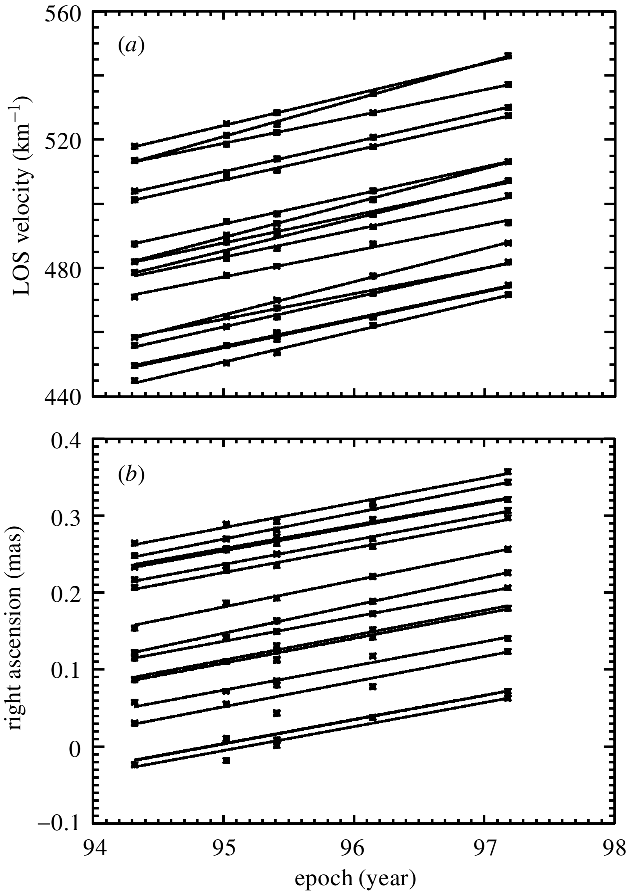

Figure 5. (*a*) Line-of-sight (LOS) velocities of selected features in the systemic group of masers in NGC 4258. The lines show the best-fitting accelerations derived from a Bayesian analysis. (*b*) The right ascension of selected maser features. The scatter in the slopes of the velocity and position curves is due to noise and actual variations in the annular radii of the features. From Herrnstein *et al*. (1999).

The cause of the warp is unknown, but several suggestions have been put forward. Papaloizou *et al*. (1998) show that the warp could be produced by a binary companion orbiting outside the maser disc. Its mass would need to be comparable with the mass of the disc (less than $10^6\ M_\odot$, based on possible deviations from Keplerian motion around a central mass). Alternatively, radiation pressure from the central source will produce torques on a slightly warped disc and will cause the warp to grow (Maloney *et al*. 1996).

Finally, it is conceivable that in the absence of other torques, the observed warp is due to the Lense–Thirring effect. A maximally rotating black hole will cause a precession of a non-aligned orbit (weak field limit) of

$$\Omega_{\mathrm{LT}} = \frac{2G^2M^2}{c^3R^3}. \tag{6.1}$$

At the inner radius of the disc ($R/R_\mathrm{S} = 40\,000$), the precession amounts to $3\times$

Table 2. *Water masers with resolved structure*

(Symbols: D, distance (Mpc); v_o, systemic velocity (km s^{-1}); Δv, velocity range (km s^{-1}); ΔR, linear extent (pc); v_ϕ, rotational velocity (km s^{-1}); R_i/R_o, inner/outer radius of disc (pc); M, central mass ($10^6\ M_\odot$); ρ, central mass density ($10^7\ M_\odot\ \mathrm{pc}^{-3}$); L_X, X-ray luminosity (10^{42} erg s^{-1}).)

(Notes: [a]L. J. Greenhill *et al.* (unpublished data); [b]Claussen *et al.* (1998); [c]Nakai *et al.* (1998); [d]Miyoshi *et al.* (1995); [e]Greenhill & Gwinn (1997); [f]L. J. Greenhill *et al.* (unpublished data); [g]Greenhill *et al.* (1997); [h]J. A. Braatz *et al.* (unpublished data); [i]Trotter *et al.* (1998), Satoh *et al.* (1998).)

masers without obvious disc structure					
galaxy	D	v_o	Δv	ΔR	comment
IRAS 22265 (S0)[a]	100	7570	150	2.4	messy
NGC 1052 (E4)[b]	20	1490	100	0.6	'jet'
IC 2560[c]	38	2900	30	0.2	velocity gradient

masers with disc structure						
galaxy	D	v_ϕ	R_i/R_o	M	ρ	L_X
NGC 4258[d]	7	1100	0.13/0.26	39	400	0.04
NGC 1068[e]	15	330	0.6/1.2	17	3	40
Circinus[f]	4	230	0.08/0.8	1	40	40
NGC 4945[g]	4	150	0.2/0.4	1	2	1
NGC 1386[h]	12	100	—/0.7	2	4	0.02
NGC 3079[i]	16	150	—/1.0	1	0.2	0.02

10^{-17} s^{-1}. This precession is very small but it might be significant over the lifetime of the disc. The measured limit on H/R and the standard accretion model together give an estimate of the time for inflowing material to cross the maser disc of *ca.* 10^{16} s for $\alpha = 0.1$, which would produce a differential precession of *ca.* $10°$ across the radius of the disc. If the axis of the disc is inclined with respect to the axis of the black hole, then the viscosity of the disc is expected to twist the plane of the innermost part of the disc toward the equatorial plane of the black hole (Bardeen & Petterson 1975; Kumar & Pringle 1985).

7. Masers in other AGN

As of mid-1999, 22 masers had been detected among about 700 galaxies searched (see, for example, Braatz *et al.* 1997). The yield rate of detections is only *ca.* 3%. The major reason for this paucity is probably that the maser discs can only be seen if they are edge-on to the line of sight. If the typical beam angle, β, is $8°$, as in NGC 4258, then the probability of seeing a maser is about equal to $\sin\beta$, or 8%. Braatz *et al.* (1997) have shown that most of the known masers are associated with Seyfert II galaxies or LINERs where the accretion discs are thought to be edge-on to the Earth.

It is difficult to make VLBI measurements on masers weaker than *ca.* 0.5 Jy because of the need to detect the maser within the coherence time of the interferometer. Nine masers have been studied with VLBI. Four of these show strong evidence of disc structure, and two more show probable disc structure. The properties of these masers are listed in table 2. Unfortunately, none of these masers shows the kind of simple, well-defined structure that would make them useful for precise study of the physical properties of accretion discs around black holes.

8. Opportunities for the future

The measurements of the positions and velocities of the masers in the nucleus of NGC 4258 offer compelling evidence for the existence of a supermassive black hole and provide the first direct image of an accretion disc within $10^5 R_S$ of a black hole. Much more can be learned from this system. A measurement of the disc thickness is important and may require higher signal-to-noise ratios than are achievable currently or VLBI measurements from space. Measurement of the continuum spectrum from the central region is very important to the understanding of the radiation process. Detection of radio emission would require instruments of higher sensitivity. Continued measurements over time of the positions and velocities of the masers will refine the estimates of their proper motions and accelerations, and this will better define the shape of the disc. It is even conceivable that the radial drift velocity will be detected. This work will benefit immensely from new instruments that are in the planning stage for centimetre-wavelength radio astronomy. These include the enhanced Very Large Array, the Square Kilometer Array and space VLBI missions such as ARISE.

I thank Ann Bragg, Lincoln Greenhill, James Herrnstein, and Adam Trotter for helpful discussions.

References

Bardeen, J. M. & Petterson, J. A. 1975 The Lense–Thirring effect and accretion disks around Kerr black holes. *Astrophys. J.* **195**, L65–L67.

Braatz, J. A., Wilson, A. S. & Henkel, C. 1997 A survey for H_2O megamasers in active galactic nuclei. II. A comparison of detected and undetected galaxies. *Astrophys. J. Suppl.* **110**, 321–346.

Bragg, A. E., Greenhill, L. J., Moran, J. M. & Henkel, C. 2000 Accelerations of water masers in NGC 4258. *Astrophys. J.* (In the press.)

Cecil, G., Wilson, A. S. & Tully, R. B. 1992 The braided jets in the spiral galaxy NGC 4258. *Astrophys. J.* **390**, 365–377.

Claussen, M. J., Diamond, P. J., Braatz, J. A., Wilson, A. S. & Henkel, C. 1998 The water masers in the elliptical galaxy NGC 1052. *Astrophys. J.* **500**, L129–L132.

Deguchi, S. & Watson, W. D. 1989 Interacting masers and the extreme brightness of astrophysical water masers. *Astrophys. J.* **340** L17–L20.

Fiebig, D. & Güsten, R. 1989 Strong magnetic fields in interstellar H_2O maser clumps. *Astron. Astrophys.* **214**, 333–338.

Frank, J., King, A. & Raine, D. 1992 *Accretion power in astrophysics.* Cambridge University Press.

Gammie, C. F., Narayan, R. & Blandford, R. 1999 What is the accretion rate in NGC 4258? *Astrophys. J.* **516**, 177–186.

Greenhill, L. J. & Gwinn, C. R. 1997 VLBI imaging of water maser emission from a nuclear disk in NGC 1068. *Astrophys. Space Sci.* **248**, 261–267.

Greenhill, L. J., Henkel, C., Becker, R., Wilson, T. L. & Wouterloot, J. G. A. 1995 Centripetal acceleration within the subparsec nuclear maser disk of NGC 4258. *Astron. Astrophys.* **304**, 21–33.

Greenhill, L. J., Moran, J. M. & Herrnstein, J. R. 1997 The distribution of H_2O maser emission in the nucleus of NGC 4258. *Astrophys. J.* **481**, L23–L26.

Haschick, A. D., Baan, W. A. & Peng, E. W. 1994 The masering torus in NGC 4258. *Astrophys. J.* **437**, L35–L38.

Herrnstein, J. R. 1996 Observations of the sub-parsec maser disk in NGC 4258. PhD thesis, Harvard University.

Herrnstein, J. R., Greenhill, L. J. & Moran, J. M. 1996 The warp in the subparsec molecular disk in NGC 4258 as an explanation for persistent asymmetries in the maser spectrum. *Astrophys. J.* **468**, L17–L20.

Herrnstein, J. R., Moran, J. M., Greenhill, L. J., Diamond, P. J., Miyoshi, M., Nakai, N. & Inoue, M. 1997 Discovery of a subparsec jet 4000 Schwarzschild radii away from the central engine of NGC 4258. *Astrophys. J.* **475**, L17–L20.

Herrnstein, J. R., Moran, J. M., Greenhill, L. J., Blackman, E. G. & Diamond, P. J. 1998*a* Polarimetric observations of the masers in NGC 4258: an upper limit on the large-scale magnetic field 0.2 parsecs from the central engine. *Astrophys. J.* **508**, 243–247.

Herrnstein, J. R., Greenhill, L. J., Moran, J. M., Diamond, P. J., Inoue, M., Nakai, N. & Miyoshi, M. 1998*b* VLBA continuum observations of NGC 4258: constraints on an advection-dominated accretion flow. *Astrophys. J.* **497**, L69–L73.

Herrnstein, J. R., Moran, J. M., Greenhill, L. J., Diamond, P. J., Inoue, M., Nakai, N., Miyoshi, M., Henkel, C. & Riess, A. 1999 A geometric distance to the galaxy NGC 4258 from orbital motions in a nuclear gas disk. *Nature* **400**, 539–541.

Kumar, S. & Pringle, J. E. 1985 Twisted accretion discs: the Bardeen–Petterson effect. *Mon. Not. R. Astron. Soc.* **213**, 435–442.

Madore, B. F., *et al.* 1999 The Hubble Space Telescope Key Project on the extragalactic distance scale. XV. A Cepheid distance to the Fornax Cluster and its implications. *Astrophys. J.* **515**, 29–41.

Makishima, K., Fujimoto, R., Ishisaki, Y., Kü, T., Lowenstein, M., Mushotzky, R., Serlemitsos, P., Sonobe, T., Tashiro, M. & Yaqoob, T. 1994 Discovery of an obscured low luminosity active nucleus in the spiral galaxy NGC 4258. *Publ. Astron. Soc. Jap.* **46**, L77–L80.

Maloney, P. R., Begelman, M. C. & Pringle, J. E. 1996 Radiation-driven warping: the origin of warps and precession in accretion disks. *Astrophys. J.* **472**, 582–587.

Maoz, E., Newman, J. A., Ferrarese, L., Stetson, P. B., Zepf, S. E., Davis, M., Freedman, W. L. & Madore, B. F. 1999 A distance to the galaxy NGC 4258 from observations of Cepheid variable stars. *Nature* **401**, 351–354.

Michell, J. 1784 On the means of discovering the distance, magnitude, etc., of the fixed stars, in consequence of the diminution of the velocity of their light. *Phil. Trans. R. Soc. Lond.* **74**, 35–37.

Miyoshi, M., Moran, J., Herrnstein, J., Greenhill, L., Nakai, N., Diamond, P. & Inoue, M. 1995 Evidence for a massive black hole from high rotation velocities in a sub-parsec region of NGC 4258. *Nature* **373**, 127–129.

Moran, J. M., Papadopoulos, G. D., Burke, B. F., Lo, K. Y., Schwartz, P. R. & Thacker, D. L. 1973 Very long baseline interferometric observations of the H_2O sources in W49 N, W3(OH), Orion A, and VY Canis Majoris. *Astrophys. J.* **185**, 535–567.

Moran, J., Greenhill, L., Herrnstein, J., Diamond, P., Miyoshi, M., Nakai, N. & Inoue, M. 1995 Probing active galactic nuclei with H_2O megamasers. *Proc. Natn. Acad. Sci. USA* **92**, 11 427–11 433.

Moran, J. M., Greenhill, L. J. & Herrnstein, J. R. 2000 Observational evidence for massive black holes in the centers of active galaxies. *J. Astron. Astrophys.* (In the press.)

Nakai, N., Inoue, M., Miyazawa, K., Miyoshi, M. & Hall, P. 1995 Search for extremely-high-velocity H_2O maser emission in Seyfert galaxies. *Publ. Astron. Soc. Jap.* **47**, 771–799.

Nakai, N., Inoue, M., Hagiwara, Y., Miyoshi, M. & Diamond, P. J. 1998 VLBI observations of a megamaser in a Seyfert galaxy IC 2560. In *Radio emission from galactic and extragalactic compact sources* (ed. J. A. Zensus, G. B. Taylor & J. M Wrobel), vol. 144, pp. 237–238. San Francisco, CA: ASP.

Nedoluha, G. E. & Watson, W. D. 1992 The Zeeman effect in astrophysical water masers and the observation of strong magnetic fields in regions of star formation. *Astrophys. J.* **384**, 185–196.

Neufeld, D. A. & Maloney, P. R. 1995 The mass accretion rate through the masing molecular disk in the active galaxy NGC 4258. *Astrophys. J.* **447**, L17–L20.

Papaloizou, J. C. B., Terquem, C. & Lin, D. N. C. 1998 On the global warping of a thin self-gravitating near-Keplerian gaseous disk with application to the disk in NGC 4258. *Astrophys. J.* **497**, 212–226.

Satoh, S., Inoue, M., Nakai, N., Shibata, K. M., Kameno, S., Migenes, V. & Diamond, P. J. 1998 Global VLBA observations of NGC 3079. In *Highlights of astronomy* (ed. J. Andersen), vol. 11B, pp. 972–973. Dordrecht: Kluwer.

Shakura, N. I. & Sunyaev, R. A. 1973 Black holes in binary systems: observational appearance. *Astron. Astrophys.* **24**, 337–355.

Stanek, K. Z., Kaluzny, J., Wysocka, A. & Thompson, I. 2000 UBVI color-magnitude diagrams in Baade's window: metallicity range and the implications for the red clump method and the distance to the Large Magellanic Cloud. *Astronom. Jl.* (In the press.)

Trotter, A. S., Greenhill, L. J., Moran, J. M., Reid, M. J., Irwin, J. A. & Lo, K. Y. 1998 Water maser emission and the parsec-scale jet in NGC 3079. *Astrophys. J.* **495**, 740–748.

Walker, R. C. 1984 H_2O in W49N. II. Statistical studies of hyperfine structure, clustering, and velocity distributions. *Astrophys. J.* **280**, 618–628.

Discussion

A. Shukurov (*University of Newcastle, UK*). A brief comment about your upper limits of the magnetic field strength—actually, the field strength at these densities and temperatures is 0.1 G, so the upper limits you have just mentioned imply that the field is weaker than the equipartition value, which is fairly consistent with what you might expect.

J. M. Moran. Our firm magnetic field limit is 0.3 G, so there may be equipartition of energy. However, we only have upper limits for density and temperature.